Inorganic Chemistry
Article

Inorg. Chem. **2009**, *48*, 9345–9355 **9345**
DOI: 10.1021/ic901248r

Magnetic and ^{57}Fe Mössbauer Study of the Single Molecule Magnet Behavior of a Dy_3Fe_7 Coordination Cluster

Ghulam Abbas,[†] Yanhua Lan,[†] Valeriu Mereacre,[†] Wolfgang Wernsdorfer,[‡] Rodolphe Clérac,[§,∥] Gernot Buth,[⊥] Moulay T. Sougrati,[#] Fernande Grandjean,[#] Gary J. Long,[*,▽] Christopher E. Anson,[†] and Annie K. Powell[*,†]

[†]*Institut für Anorganische Chemie, Karlsruhe Institute of Technology, University of Karlsruhe, Engesserstrasse 15, D-76131 Karlsruhe, Germany,* [‡]*Institut Néel CNRS, BP 166, 25 avenue des Martyrs, F-38042 Grenoble, France,* [§]*CNRS, UPR 8641, Centre de Recherche Paul Pascal Equipe "Matériaux Moléculaires Magnétiques", 115 avenue du Dr. Albert Schweitzer, F-33600 Pessac, France,* [∥]*Université de Bordeaux, UPR 8641, F-33600, Pessac, France,* [⊥]*Institut für Synchrotronstrahlung, Karlsruhe Institute of Technology, Forschungszentrum Karlsruhe, D-76344 Eggenstein-Leopoldshafen, Germany,* [#]*Department of Physics, University of Liège, B-4000 Sart-Tilman, Belgium, and* [▽]*Department of Chemistry, Missouri University of Science and Technology, University of Missouri, Rolla, Missouri 65409-0010*

Received June 29, 2009

The reaction between *N*-methydiethanolamine ($mdeaH_2$), benzoic acid, $FeCl_3$, and $DyCl_3$ yields a decanuclear coordination cluster, $[Dy_3Fe_7(\mu_4\text{-}O)_2(\mu_3\text{-}OH)_2(mdea)_7(\mu\text{-benzoate})_4(N_3)_6]\cdot 2H_2O\cdot 7CH_3OH$ (**1**) whose single crystal structure exhibits three and seven crystallographically distinct Dy(III) and Fe(III) ions; six of the Fe(III) ions are *pseudo*-octahedrally coordinated, whereas the seventh has a trigonal-bipyramidal coordination geometry. Both direct current (*dc*) and alternating current (*ac*) magnetic susceptibility studies indicate that, upon cooling, intracluster antiferromagnetic interactions are dominant in **1**, yielding a ferrimagnetic spin arrangement. The out-of-phase (χ'') *ac* susceptibility reveals that **1** undergoes a slow relaxation of its magnetization mainly resulting from the anisotropy of the Dy(III) ions. This slow relaxation has been confirmed both by magnetization measurements on an oriented single crystal of **1** and by the observation of hysteresis loops below 1.9 K. The macroscopic magnetic studies yield an effective energy barrier, U_{eff}, of 33.4 K for this relaxation, a barrier that is the highest yet reported for a lanthanide(III)-Fe(III) single molecule magnet. The ^{57}Fe Mössbauer spectra of **1** obtained between 3 and 35 K are consistent with the presence of Fe(III) intracluster antiferromagnetic coupling with slow magnetic relaxation relative to the Larmor precession time, thus confirming, on a microscopic scale, the presence of a barrier to the magnetic relaxation below 35 K. Between 55 and 295 K the Mössbauer spectra reveal paramagnetic behavior with six partially resolved quadrupole doublets, one for the trigonal-bipyramidal Fe(III) site and five for the six *pseudo*-octahedral Fe(III) sites.

Introduction

The discovery of the first single molecule magnet[1] has generated new interest in the field of magnetism because single molecule magnets may be magnetized below a certain temperature with retention of their magnetization upon removal of the applied magnetic field.[2−4] To date the quest for new 4f-3d single molecule magnets displaying high blocking temperatures has focused on heterometallic complexes that combine the large, predominately anisotropic, magnetic moments of lanthanide(III) ions with the high spin-states of many transition metal ions. Thus coordination complexes containing a combination of lanthanide(III) ions with manganese(II,III,IV),[5]

*To whom correspondence should be addressed. E-mail: powell@aoc.uni-karlsruhe.de (A.P.), glong@mst.edu (G.J.L.). Phone: +49-721-608-2135 (A.P.). Fax: +49-721-608-8142 (A.P.).

(1) (a) Lis, T. *Acta Crystallogr., Sect. B* **1980**, *36*, 2042. (b) Boyd, P. D. W.; Li, Q.; Vincent, J. B.; Folting, K.; Chang, H.-R.; Streib, W. E.; Huffman, J. C.; Christou, G.; Hendrickson, D. N. *J. Am. Chem. Soc.* **1988**, *110*, 8537. (c) Caneschi, A.; Gatteschi, D.; Sessoli, R. *J. Am. Chem. Soc.* **1991**, *113*, 5873. (d) Sessoli, R.; Tsai, H.-L.; Schake, A. R.; Wang, S.; Vincent, J. B.; Folting, K.; Gatteschi, D.; Christou, G.; Hendrickson, D. N. *J. Am. Chem. Soc.* **1993**, *115*, 1804. (e) Sessoli, R.; Gatteschi, D.; Caneschi, A.; Novak, M. A. *Nature* **1993**, *365*, 141.

(2) (a) Gatteschi, D.; Sessoli, R.; Cornia, A. *Chem. Commun.* **2000**, 725. (b) Christou, G.; Gatteschi, D.; Hendrickson, D. N.; Sessoli, R. *MRS Bull.* **2000**, *25*, 66.

(3) Gatteschi, D.; Sessoli, R. *Angew. Chem., Int. Ed.* **2003**, *42*, 268.

(4) Wernsdorfer, W.; Aliaga-Alcalde, N.; Hendrickson, D. N.; Christou, G. *Nature* **2006**, *416*, 406.

(5) (a) Benelli, C.; Murrie, M.; Parsons, S.; Winpenny, R. *J. Chem. Soc., Dalton Trans.* **1999**, 4125. (b) Zaleski, C.; Depperman, E.; Kampf, J.; Kirk, M.; Pecoraro, V. *Angew. Chem., Int. Ed.* **2004**, *43*, 3912. (c) Mishra, A.; Wernsdorfer, W.; Abboud, K.; Christou, G. *J. Am. Chem. Soc.* **2004**, *126*, 15648. (d) Mishra, A.; Wernsdorfer, W.; Parsons, S.; Christou, G.; Brechin, E. *Chem. Commun.* **2005**, 2086. (e) Mereacre, V.; Ayuk Ako, M.; Clérac, R.; Wernsdorfer, W.; Filoti, G.; Bartolomé, J.; Anson, C. E.; Powell, A. K. *J. Am. Chem. Soc.* **2007**, *129*, 9248. (f) Mereacre, V.; Ayuk Ako, M.; Clérac, R.; Wernsdorfer, W.; Hewitt, I. J.; Anson, C. E.; Powell, A. K. *Chem.—Eur. J.* **2008**, *14*, 3577. (g) Stamatotos, Th. C.; Teat, S. J.; Wernsdorfer, W.; Christou, G. *Angew. Chem., Int. Ed.* **2009**, *48*, 521. (h) Ayuk Ako, M.; Mereacre, V.; Clérac, R.; Wernsdorfer, W.; Hewitt, I. J.; Anson, C. E.; Powell, A. K. *Chem. Commun.* **2009**, 544.

Published on Web 08/27/2009

iron(II,III),[6,7,8a] cobalt(II),[9] nickel(II),[10] and copper(II)[11−13] ions have been investigated in recent years. For example, the Dy_3Cu_6 and $GdCo_2$ complexes have recently been reported[12c,9] to have effective magnetization reversal energy barriers, U_{eff}, of about 25 to 28 K. Similarly, the combination of lanthanide(III) and Mn(III) and Mn(IV) ions has yielded[5f] a U_{eff} of 38 K, one of the highest energy barriers yet reported for the relaxation of the magnetization in a 4f-3d single molecule magnet. The magnetic interactions in these compounds are more complex than in those containing only 3d metal ions. With the exception of the isotropic Gd(III) ion and the diamagnetic La(III) and Lu(III) ions, the ground states of the remaining lanthanide(III) ions have an orbital angular momentum, which prevents modeling the magnetism with a spin-only Hamiltonian for isotropic exchange. However, by using Gd(III) in a complex the lanthanide anisotropy and orbital angular momentum can be "turned off," whereas with La(III) and Lu(III) the 4f contribution to the magnetism can be completely removed. In the case of a Eu(III) ion, which has a $J = 0$ diamagnetic ground state, the interpretation of the magnetic properties is also complicated by the presence of low lying $J \neq 0$ excited states that produce a paramagnetic contribution to the moment that can hide any magnetic exchange coupling.

Alkoxy ligands have been widely employed in the synthesis of high nuclearity clusters because they possess both chelating and bridging capabilities.[14] Although significant progress has been made in the use of diethanolamine and related tripodal ligands in the synthesis of high-spin manganese[15a−15c] and high nuclearity iron[15d−15f] and nickel[15d] complexes, there has been much less progress in preparing mixed-metal clusters derived from these ligands.[5f,6b,8,16] The possibility of using aminopolyalcohol based ligands was encouraging because the hard-donor oxygen tends to bind to oxophilic lanthanide ions and the soft-donor nitrogen tends to bind to transition-metal ions. Further, the deprotonated hydroxyethyl portions of these ligands are very good bridging groups and favor the formation of high nuclearity coordination clusters. As an extension of our previous work on the synthesis of iron-lanthanide ion clusters,[8a,17] herein we employ *N*-methyldiethanolamine, $mdeaH_2$, as a ligand. Although this ligand has been used in coordination chemistry of transition metal ions in recent years,[14a,15e,15f] examples of $mdeaH_2$ acting as ligand in 4f-3d heterometal clusters are still rare.[5f] It therefore seemed logical to extend the work on the synthesis of transition metals complexes using this ligand to the synthesis of new heterometallic Fe(III) containing 4f-3d clusters. Moreover, to date we know of only three examples of dysprosium−iron cluster single molecule magnets.[6]

Herein, we report the synthesis, structure, magnetic, and Mössbauer spectral properties of $[Dy_3Fe_7(\mu_4\text{-}O)_2(\mu_3\text{-}OH)_2(mdea)_7(\mu\text{-benzoate})_4(N_3)_6]\cdot 2H_2O\cdot 7CH_3OH$, **1**, which has an effective energy barrier of 33.4 K.

Experimental Section

Synthesis. Unless otherwise stated, all reagents were obtained from commercial sources and were used as received without further purification. All reactions were carried out under aerobic conditions.

$[Dy_3Fe_7(\mu_4\text{-}O)_2(\mu_3\text{-}OH)_2(mdea)_7(\mu\text{-benzoate})_4(N_3)_6]\cdot 2H_2O\cdot 7CH_3OH$, **1**, was prepared as follows. A solution of *N*-methyldiethanolamine (0.09 g, 0.75 mmol) in 20 mL of MeOH was added dropwise over 20 min to a stirred solution of $DyCl_3\cdot 6H_2O$ (0.07 g, 0.25 mmol), benzoic acid (0.06 g, 0.50 mmol), $FeCl_3$ (0.08 g, 0.50 mmol), and NaN_3 (0.034 g, 0.50 mmol) in 20 mL of

(6) (a) Ferbinteanu, M.; Kajiwara, T.; Choi, K.-Y.; Nojiri, H.; Nakamoto, A.; Kojima, N.; Cimpoesu, F.; Fujimura, Y.; Takaishi, S.; Yamashita, M. *J. Am. Chem. Soc.* **2006**, *128*, 9008. (b) Murugesu, M.; Mishra, A.; Wernsdorfer, W.; Abboud, K.; Christou, G. *Polyhedron* **2006**, *26*, 613. (c) Pointillart, F.; Bernot, K.; Sessoli, R.; Gatteschi, D. *Chem.—Eur. J.* **2007**, *13*, 1602.

(7) (a) Costes, J. P.; Dupuis, A.; Laurent, J. P. *Eur. J. Inorg. Chem.* **1998**, 1543. (b) Costes, J. P.; Dahan, F.; Dumestre, F.; Clemente-Juan, J. M.; Garcia-Tojal, J.; Tuchagues, J. P. *Dalton Trans.* **2003**, 464. (c) Figuerola, A.; Diaz, C.; Ribas, J.; Tangoulis, V.; Granell, J.; Lloret, F.; Mahia, J.; Maestro, M. *Inorg. Chem.* **2003**, *42*, 641. (d) Shova, S. G.; Turta, C. I.; Simonov, Yu.; Gdaniec, M.; Prodius, D. N.; Mereacre, V. M. *Acta Crystallogr.* **2004**, *A60*, s271. (e) Turta, C. I.; Prodius, D. N.; Mereacre, V. M.; Shova, S. G.; Gdaniec, M.; Simonov, Yu. A.; Kuncser, V.; Filoti, G.; Caneschi, A.; Sorace, L. *Inorg. Chem. Commun.* **2004**, *7*, 576.

(8) (a) Ako, A. M.; Mereacre, V.; Clérac, R.; Hewitt, I. J.; Lan, Y.; Anson, C. E.; Powell, A. K. *Dalton Trans.* **2007**, 5245. (b) Saalfrank, R. W.; Prakash, R.; Maid, H.; Hampel, F.; Heinemann, F. W.; Trautwein, A. X.; Böttger, L. H. *Chem.−Eur. J.* **2006**, *12*, 2428.

(9) Chandrasekhar, V.; Pandian, B. M.; Azhakar, R.; Vittal, J. J.; Clérac, R. *Inorg. Chem.* **2007**, *46*, 5140.

(10) (a) Brechin, E.; Harris, S.; Parsons, S.; Winpenny, R. *J. Chem. Soc., Dalton Trans.* **1997**, 1665. (b) Costes, J.-P.; Dahan, F.; Dupuis, A.; Laurent, J.-P. *Inorg. Chem.* **1997**, *36*, 4284. (c) Shiga, T.; Ito, N.; Hidaka, A.; Okawa, H.; Kitagawa, S.; Ohba, M. *Inorg. Chem.* **2007**, *46*, 3492. (d) Madalan, A. M.; Avarvari, N.; Fourmiguè, M.; Clérac, R.; Chibotaru, L. F.; Clima, S.; Andruh, M. *Inorg. Chem.* **2007**, *47*, 940.

(11) (a) Costes, J.-P.; Clemente-Juan, J.-M.; Dahan, F.; Milon, J. *Inorg. Chem.* **2004**, *43*, 8200. (b) Costes, J.-P.; Dahan, F.; Wernsdorfer, W. *Inorg. Chem.* **2006**, *45*, 5. (c) Mori, F.; Nyui, T.; Ishida, T.; Nogami, T.; Choi, K.-Y.; Nojiri, H. *J. Am. Chem. Soc.* **2006**, *128*, 1440. (d) Osa, S.; Kido, T.; Matsumoto, N.; Re, N.; Pochaba, A.; Mrozinski, J. *J. Am. Chem. Soc.* **2004**, *126*, 420. (e) Aronica, C.; Pilet, G.; Chastanet, G.; Wernsdorfer, W.; Jacquot, J.-F.; Luneau, D. *Angew. Chem., Int. Ed.* **2006**, *45*, 4659. (f) Novitchi, Gh.; Costes, J.-P.; Tuchagues, J.-P.; Vendier, L.; Wernsdorfer, W. *New J. Chem.* **2008**, *32*, 197. (g) Novitchi, Gh.; Wernsdorfer, W.; Chibotaru, L.; Costes, J.-P.; Anson, C. E.; Powell, A. K. *Angew. Chem., Int. Ed.* **2009**, *48*, 1614.

(12) (a) Bencini, A.; Benelli, C.; Caneschi, A.; Carlin, R. L.; Dei, A.; Gatteschi, D. *J. Am. Chem. Soc.* **1985**, *107*, 8128. (b) Andruh, M.; Ramade, I.; Codjovi, E.; Guillou, O.; Kahn, O.; Trombe, J. C. *J. Am. Chem. Soc.* **1993**, *115*, 1822. (c) Aronica, C.; Pilet, G.; Chastanet, G.; Wernsdorfer, W.; Jacquot, J.-F.; Luneau, D. *Angew. Chem., Int. Ed.* **2006**, *45*, 4659.

(13) (a) Kahn, M. L.; Mathonière, C.; Kahn, O. *Inorg. Chem.* **1999**, *38*, 3692. (b) Sutter, J.-P.; Kahn, M. L.; Kahn, O. *Adv. Mater.* **1999**, *11*, 863. (c) Kahn, M. L.; Sutter, J.-P.; Golhen, S.; Guionneau, P.; Ouahab, L.; Kahn, O.; Chasseau, D. *J. Am. Chem. Soc.* **2000**, *122*, 3413. (d) Kahn, M. L.; Lecante, P.; Verelst, M.; Mathonière.; Kahn, O. *Chem. Mater.* **2000**, *12*, 3073. (e) Kahn, M. L.; Ballou, R.; Porcher, P.; Kahn, O.; Sutter, J.-P. *Chem.—Eur. J.* **2002**, *8*, 525.

(14) (a) Rumberger, E. M.; Shah, S. J.; Beedle, C. C.; Zakharov, L. N.; Rheingold, A. L.; Hendrickson, D. N. *Inorg. Chem.* **2005**, *44*, 2742. (b) Murugesu, M.; Habrych, M.; Wernsdorfer, W.; Abboud, K. A.; Christou, G. *J. Am. Chem. Soc.* **2004**, *126*, 4766. (c) Boskovic, C.; Wernsdorfer, W.; Folting, K.; Huffmann, J. C.; Hendrickson, D. N.; Christou, G. *Inorg. Chem.* **2002**, *41*, 5107. (d) Glaser, T.; Liratzis, I.; Lügger, T.; Fröhlich, R. *Eur. J. Inorg. Chem.* **2004**, 2683. (e) Yang, C. I.; Lee, G. H.; Wur, C. S.; Lin, J. G.; Tsai, H. L. *Polyhedron* **2005**, *24*, 2215. (f) Saalfrank, R. W.; Nakajima, T.; Mooren, N.; Scheurer, A.; Maid, H.; Hampel, F.; Trieflinger, C.; Daub, J. *Eur. J. Inorg. Chem.* **2005**, 1149.

(15) (a) Saalfrank, R. W.; Scheurer, A.; Prakash, R.; Heinemann, F. W.; Nakajima, T.; Hampel, F.; Leppin, R.; Pilawa, B.; Rupp, H.; Müller, P. *Inorg. Chem.* **2007**, *46*, 1586. (b) Manoli, M.; Prescimone, A.; Bagai, R.; Mishra, A.; Murugesu, M.; Parsons, S.; Wernsdorfer, W.; Christou, G.; Brechin, E. K. *Inorg. Chem.* **2007**, *46*, 6968. (c) Rajaraman, G.; Murugesu, M.; Sanudo, E. C.; Soler, M.; Wernsdorfer, W.; Helliwell, M.; Muryn, C.; Raftery, J.; Teat, S. J.; Christou, G.; Brechin, E. K. *J. Am. Chem. Soc.* **2004**, *126*, 15445. (d) Foguet-Albiol, D.; Abboud, K.; Christou, G. *Chem. Commun.* **2005**, 4282. (e) Saalfrank, R. W.; Deutscher, Ch.; Sperner, S.; Nakajima, T.; Ayuk Ako, M.; Uller, E.; Hampel, F.; Heinemann, F. W. *Inorg. Chem.* **2004**, *43*, 4372. (f) Saalfrank, R. W.; Maid, H.; Scheurer, A. *Angew. Chem., Int. Ed.* **2008**, *47*, 8794.

(16) Wang, W. -G.; Zhou, A.; Zhang, W. -X.; Tong, M. -L.; Chen, X. -M.; Nakano, M.; Beedle, C. C.; Hendrickson, D. N *J. Am. Chem. Soc.* **2007**, *129*, 1014.

(17) Mukherjee, S.; Lan, Y.; Novitchi, Gh.; Kostakis, G.; Anson, C. E.; Powell, A. K. *Polyhedron* **2009**, *28*, 1782.

MeOH. The mixture was heated under reflux for 1 h after which it was cooled at room temperature and then allowed to stand undisturbed in a sealed vial. Orange needles of **1** were obtained after 3 days in 40% yield. The crystals were collected by filtration and washed with MeCN.

Elemental analysis (%) calcd (found) for $Dy_3Fe_7C_{63}H_{103}N_{25}O_{28}$ (corresponds to loss of the 7 lattice methanols): C, 29.82 (29.95); H, 4.09 (3.95); N, 13.80 (13.81). IR (KBr): ν (cm^{-1}) = 3421 (w), 2851 (w), 2059 (vs), 1594 (w), 1548 (m), 1400 (s), 1259 (w), 1085 (m), 1026 (w), 1000 (w), 898 (w), 721 (m), 655(w), 578 (w), 491 (w).

X-ray Crystallography. X-ray crystallographic data for **1** were collected on a Bruker SMART Apex CCD diffractometer using graphite-monochromated Mo Kα radiation. Crystals of **1** twin by a 180° rotation about *c**; data were integrated as a twin and corrected for absorption using TWINABS.[18b] The structure was solved using direct methods, followed by full-matrix least-squares refinement against F^2 (all data, *HKLF* 5 format) using SHELXTL.[18a] Anisotropic refinement was used for all ordered non-H atoms; organic H atoms were placed in calculated positions.

Crystal data for **1**: $Dy_3Fe_7C_{70}H_{131}N_{25}O_{35}$, M_r = 2761.4 g/mol, triclinic, space group $P\bar{1}$, a = 14.2482(17), b = 17.446(2), c = 21.224(2) Å, α = 90.430(2)°, β = 92.445(2)°, γ = 98.445(2)°, V = 5212.4(11) Å^3, T = 100 K, Z = 2, μ(Mo-Kα) = 3.152 mm^{-1}, $F(000)$ = 2772, ρ_{calcd} = 1.759 Mg m^{-3}. 44477 reflections measured, of which 24716 unique (R_{int} = 0.0389), 1213 parameters, final wR_2 (F^2, all data) = 0.1753, S = 1.071, R_1 (19922 with $I > 2\sigma(I)$) = 0.0551. Crystallographic data (excluding structure factors) for the structures in this paper have been deposited with the Cambridge Crystallographic Data Centre as supplementary publication no. CCDC 729433. Copies of the data can be obtained, free of charge, on application to CCDC, 12 Union Road, Cambridge CB2 1EZ, U.K.: http://www.ccdc.cam.ac.uk/cgi-bin/catreq.cgi, e-mail: data_request@ccdc.cam.ac.uk, or fax: +44 1223 336033.

Data for a crystal of **1** that had been exposed to the air (and lost the lattice methanols according to CHN data) were measured at 150 K on the SCD beamline of the ANKA synchrotron at the Forschungszentrum Karlsruhe, using Si-monochromated radiation of wavelength λ = 0.80000 Å. The data set was not of high quality because of high mosaicity, and the structure could not be refined to a fully publishable standard (R_1 = 0.1509). However, it was sufficient to demonstrate that the molecular structure had remained unchanged, and to reveal the change in the crystal packing on desolvation. Triclinic, space group $P\bar{1}$, a = 14.447(2), b = 17.000(4), c = 21.277(3) Å, α = 108.962(14)°, β = 99.885(12)°, γ = 96.484(14)°, V = 4788.4(14) Å^3.

Physical Measurements. Elemental analyses for C, H, and N were performed using an Elementar Vario EL analyzer at the Institute of Inorganic Chemistry, University of Karlsruhe. IR spectra were measured on a Perkin-Elmer *Spectrum One* spectrometer as KBr disks.

Magnetic susceptibility measurements were obtained with a Quantum Design SQUID magnetometer MPMS-XL. Magnetization measurements on single crystals were performed with an array of micro-SQUIDs.[19] The SQUID measurements were performed on polycrystalline samples, first as 7.5 mg of powder placed in a plastic bag and, second, as 6.6 mg of powder restrained in ~6.0 mg of grease. Alternating current (*ac*) susceptibility measurements were performed with an oscillating *ac* field of 3 Oe and *ac* frequencies ranging from 1 to 1500 Hz. *M* versus *H* measurements were performed at 100 K to check for the presence of ferromagnetic impurities; none were observed. The magnetic data were corrected for the sample holder and the diamagnetic contribution.

For measurements between 295 and 4.2 K the Mössbauer spectral absorber contained 18 mg/cm^2 of a finely powdered sample of **1** dispersed in boron nitride; for the 3 K spectrum the absorber contained 65 mg/cm^2 of finely ground sample. The spectra were obtained between 3 and 295 K on constant acceleration spectrometers that utilized a rhodium matrix cobalt-57 source and were calibrated at room temperature with α-iron powder. The statistical errors are given in parentheses. The absolute errors for the fitted parameters are estimated to be approximately twice as large.

Results and Discussion

Synthesis. There are various strategies which have been utilized in the synthesis of iron containing 4f-3d complexes. These include among others, the self- or serendipitous assembly of preformed small nuclearity species with $[Fe_2MO]^{6+/7+}$ (M = Fe(III) or Ba(II)) cores with[6b,8a] or without[7e] chelating ligands; a successful preparation used $[Fe(bpca)_2]$, where Hbpca = bis(2-pyridylcarbonylamine) building block.[6a,6c] For other preparations, the starting materials were simple salts of iron such as $FeCl_3$.[7b]

Recently we have reported the synthesis of iron-lanthanide containing clusters by using $[Fe_3O(piv)_6(H_2O)_3](piv)$ (piv = O_2CCMe_3), which resulted in a series of high-nuclearity compounds $[Ln_8Fe^{III}_5(\mu_3\text{-}OH)_{12}(L)_4(piv)_{12}(NO_3)_4(OAc)_4]^-[H_3L]^+$.[8a] Herein, for the preparation of **1**, a variety of reaction ratios, reagents, and preparative conditions were investigated. Reaction between $FeCl_3$, $DyCl_3 \cdot 6H_2O$, benzoic acid, and *N*-methyldiethanolamine in a 2:1:2:3 molar ratio in MeOH gave a red solution from which light red crystals of $[Dy_3Fe_7(\mu_4\text{-}O)_2(\mu_3\text{-}OH)_2(mdea)_7(\mu\text{-benzoate})_4(N_3)_6] \cdot 2H_2O \cdot 7CH_3OH$, **1**, precipitated after 3 days. The same complex was also obtained, but in a much lower yield, when the $FeCl_3$ and benzoic acid were replaced by $[Fe_3O(C_6H_5CO_2)_6(H_2O)_3](C_6H_5CO_2)$. The products were identified by IR spectral comparison and elemental analysis. Small variations in the ratio of the starting materials also resulted in **1**, indicating that is the preferred product.

Crystal Structure. Compound **1** crystallizes in the triclinic space group $P\bar{1}$, with Z = 2. Although the molecule has no crystallographically imposed symmetry, an idealized 2-fold axis runs through N(1), Fe(1), and Dy(1). The central core is built up from seven Fe(III) cations, each of which is chelated by a doubly deprotonated $(mdea)^{2-}$ ligand and three Dy(III) cations. The structure of the molecule is shown in Figure 1. Two views of the central core with the benzoate and azide ligands omitted are shown in Figure 2. The bond lengths and angles are given in Table 1.

The two $(\mu_4\text{-}O)^{2-}$ ligands O(1) and O(2) each bridge between two Fe and two Dy centers, either Fe(2) and Dy(2) or Fe(3) and Dy(3), respectively, and Fe(1) and Dy(1). The resulting distorted tetrahedral $\{Fe_2Dy_2(\mu_4\text{-}O)\}$ units thus share one edge, Fe(1)···Dy(1). Within each tetrahedron, the Fe−O−Fe angles (144.1(4) and 143.5(4)°) are much larger than the Fe−O−Dy (99.1(3)−101.9(3)°) and Dy−O−Dy (106.1(2), 106.6(3)°) angles. The two Dy···Dy edges are each further bridged by a hydroxo ligand, both of which form $(\mu_3\text{-}OH)^-$ bridges to a further Fe center, with O(3) and O(4) bridging either Dy(1), Dy(2), and Fe(4), or

(18) (a) Sheldrick, G. M. *TWINABS*; University of Göttingen: Göttingen, Germany, 2005. (b) Sheldrick, G. M. *SHELXTL 6.12*; Bruker AXS Inc.: Madison, WI, 2003.

(19) Wernsdorfer, W. *Adv. Chem. Phys.* **2001**, *118*, 99.

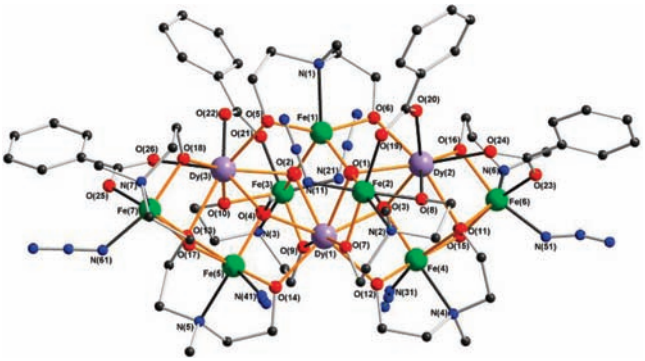

Figure 1. Molecular structure of $Dy_3Fe_7(\mu_4\text{-}O)_2(\mu_3\text{-}OH)_2(mdea)_7(\mu\text{-benzoate})_4(N_3)_6$, **1**. Organic hydrogen atoms and minor disordered components have been omitted for clarity.

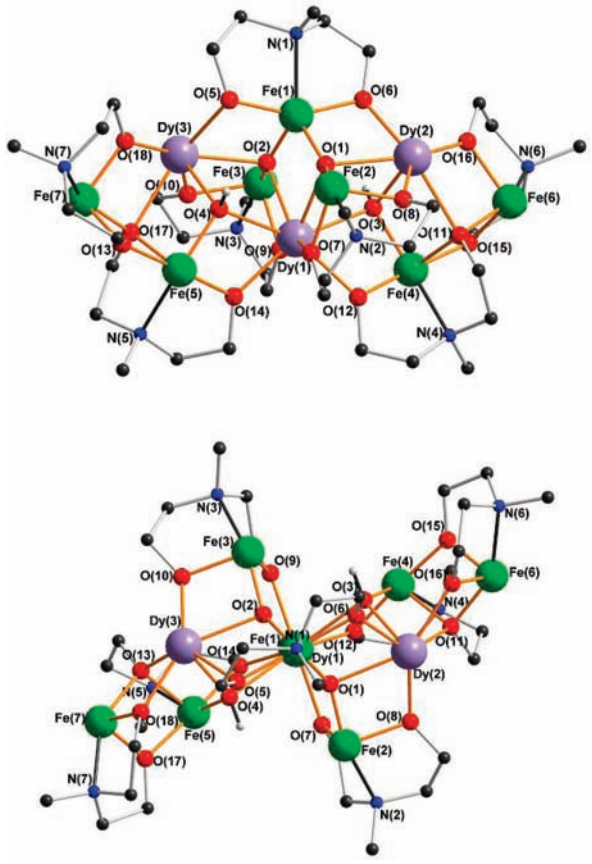

Figure 2. Two views of the structure of the core of $Dy_3Fe_7(\mu_4\text{-}O)_2(\mu_3\text{-}OH)_2(mdea)_7(\mu\text{-benzoate})_4(N_3)_6$, **1**. Azide and benzoate ligands, and C−H hydrogen atoms have been omitted for clarity.

Dy(2), Dy(3), and Fe(5), respectively. These hydroxo bridges are more regular than the oxo bridges; the angles around O(3) and O(4) are all in the range 103.0(3)−111.5(3)°. The final two triple-bridges are provided by alkoxo oxygens from two $(mdea)^{2-}$ ligands: O(13) bridges Fe(5), Dy(3), and Fe(7), while O(11) bridges Fe(4), Dy(2), and Fe(6). The angles around O(11) and O(13) are rather smaller (95.4(3)−101.6(3)°) than those for the $(\mu_3\text{-}OH)^-$ bridges. The remaining 12 $(mdea)^{2-}$ oxygens each form a (μ-OR) bridge between the iron to which their respective ligand chelates and a further metal center, thus forming 10 Fe···Dy and 2 Fe···Fe bridges. The 12 Fe−O−Dy or Fe−O−Fe angles are rather consistent; all are in the range 101.7(3)−109.9(3)°. The four benzoate ligands form *syn, syn* bridges, each between an iron and a dysprosium center.

The coordination sphere of each iron with the exception of Fe(1) is completed by a terminal azido ligand resulting in a more or less distorted *cis*-N_2O_4 octahedral environment. Fe(1) has a five-coordinate NO_4 environment in which the two alkoxo oxygens O(5) and O(6) occupy the axial sites of what is best described as a trigonal bipyramidal geometry. The Fe−O, Fe−N(azide) and Fe−N(imino) distances are in the ranges 1.880(7)−2.143(7) Å, 1.971(9)−2.080(9) Å, and 2.199(10)−2.240(10) Å, respectively. The three Dy centers are each eight-coordinate, with approximate square-antiprismatic geometries and Dy−O bond lengths in the range 2.258(8)−2.532(7) Å.

Table 1. Selected Bond Distances (Å) and Angles (deg) for **1**

Bond Lengths

Dy(1)−O(14)	2.298(7)	Fe(2)−O(19)	2.055(8)
Dy(1)−O(9)	2.298(7)	Fe(2)−N(2)	2.238(9)
Dy(1)−O(7)	2.306(7)	Fe(3)−O(2)	1.913(7)
Dy(1)−O(12)	2.334(7)	Fe(3)−O(9)	1.975(7)
Dy(1)−O(2)	2.419(7)	Fe(3)−O(10)	2.018(7)
Dy(1)−O(1)	2.433(7)	Fe(3)−O(21)	2.063(7)
Dy(1)−O(4)	2.472(7)	Fe(3)−N(21)	2.080(9)
Dy(1)−O(3)	2.499(8)	Fe(3)−N(3)	2.240(10)
Dy(2)−O(8)	2.274(7)	Fe(4)−O(12)	1.961(7)
Dy(2)−O(16)	2.317(7)	Fe(4)−O(3)	1.975(7)
Dy(2)−O(20)	2.356(8)	Fe(4)−N(31)	1.975(9)
Dy(2)−O(6)	2.359(8)	Fe(4)−O(15)	2.009(7)
Dy(2)−O(24)	2.382(8)	Fe(4)−O(11)	2.131(7)
Dy(2)−O(3)	2.401(7)	Fe(4)−N(4)	2.220(8)
Dy(2)−O(1)	2.423(7)	Fe(5)−N(41)	1.971(9)
Dy(2)−O(11)	2.532(7)	Fe(5)−O(4)	1.977(6)
Dy(3)−O(10)	2.258(8)	Fe(5)−O(14)	1.994(7)
Dy(3)−O(18)	2.272(7)	Fe(5)−O(17)	2.022(7)
Dy(3)−O(5)	2.350(8)	Fe(5)−O(13)	2.143(7)
Dy(3)−O(22)	2.358(7)	Fe(5)−N(5)	2.223(9)
Dy(3)−O(26)	2.385(8)	Fe(6)−O(16)	1.981(8)
Dy(3)−O(4)	2.419(7)	Fe(6)−O(15)	1.982(7)
Dy(3)−O(2)	2.432(7)	Fe(6)−O(23)	2.013(8)
Dy(3)−O(13)	2.524(7)	Fe(6)−N(51)	2.020(10)
Fe(1)−O(2)	1.880(7)	Fe(6)−O(11)	2.053(8)
Fe(1)−O(1)	1.905(7)	Fe(6)−N(6)	2.201(10)
Fe(1)−O(6)	1.971(7)	Fe(7)−O(18)	1.974(8)
Fe(1)−O(5)	1.974(8)	Fe(7)−O(17)	2.001(8)
Fe(1)−N(1)	2.211(6)	Fe(7)−O(25)	2.016(7)
Fe(2)−O(1)	1.890(7)	Fe(7)−N(61)	2.042(10)
Fe(2)−O(7)	1.961(7)	Fe(7)−O(13)	2.049(7)
Fe(2)−O(8)	1.994(7)	Fe(7)−N(7)	2.199(10)
Fe(2)−N(11)	2.037(9)		

Bond Angles

Dy(1)−O(2)−Dy(3)	106.6(3)	Fe(3)−O(2)−Dy(3)	99.1(3)
Dy(2)−O(1)−Dy(1)	106.1(2)	Fe(3)−O(9)−Dy(1)	104.3(3)
Dy(2)−O(3)−Dy(1)	104.7(3)	Fe(4)−O(11)−Dy(2)	101.7(3)
Dy(3)−O(4)−Dy(1)	105.4(2)	Fe(4)−O(12)−Dy(1)	109.6(3)
Fe(1)−O(1)−Dy(1)	99.1(3)	Fe(4)−O(3)−Dy(1)	103.0(3)
Fe(1)−O(1)−Dy(2)	101.6(3)	Fe(4)−O(3)−Dy(2)	111.5(3)
Fe(1)−O(2)−Dy(1)	100.3(3)	Fe(5)−O(13)−Dy(3)	101.6(3)
Fe(1)−O(2)−Dy(3)	101.7(3)	Fe(5)−O(14)−Dy(1)	109.9(3)
Fe(1)−O(2)−Fe(3)	143.5(4)	Fe(5)−O(4)−Dy(1)	104.0(3)
Fe(1)−O(5)−Dy(3)	101.7(3)	Fe(5)−O(4)−Dy(3)	110.8(3)
Fe(1)−O(6)−Dy(2)	101.8(3)	Fe(6)−O(11)−Dy(2)	95.4(3)
Fe(2)−O(1)−Dy(1)	101.8(3)	Fe(6)−O(11)−Fe(4)	101.2(3)
Fe(2)−O(1)−Dy(2)	100.1(3)	Fe(6)−O(15)−Fe(4)	108.2(3)
Fe(2)−O(1)−Fe(1)	144.1(4)	Fe(6)−O(16)−Dy(2)	104.6(3)
Fe(2)−O(7)−Dy(1)	104.1(3)	Fe(7)−O(13)−Dy(3)	95.6(3)
Fe(2)−O(8)−Dy(2)	102.1(3)	Fe(7)−O(13)−Fe(5)	101.0(3)
Fe(3)−O(10)−Dy(3)	101.9(3)	Fe(7)−O(17)−Fe(5)	107.0(3)
Fe(3)−O(2)−Dy(1)	101.9(3)	Fe(7)−O(18)−Dy(3)	106.3(3)

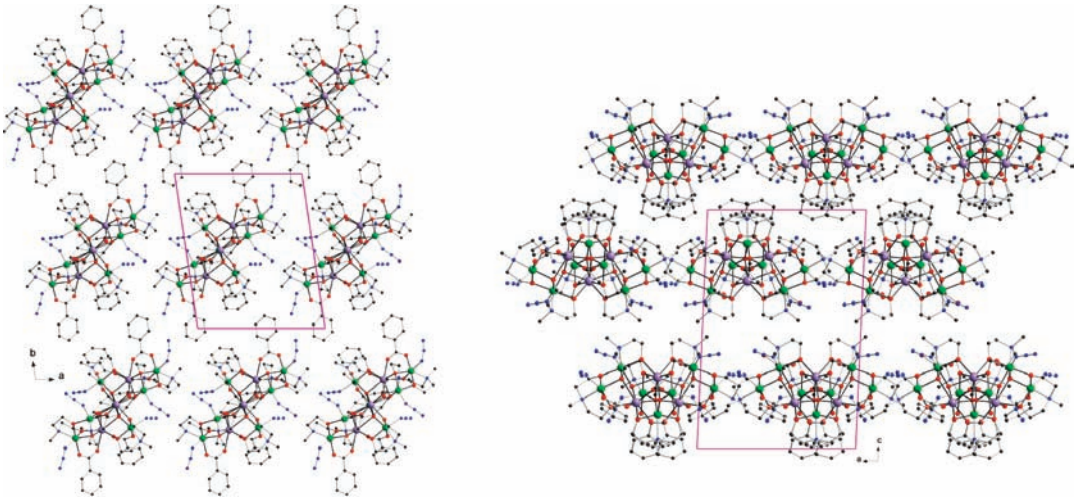

Figure 3. (left) Layer of molecules parallel to the 001 plane in the crystal structure of **1**, showing how the molecular 2-fold axes are all closely aligned to the *c* axis. (right) Crystal packing in **1** viewed along the *b* axis, emphasizing the *quasi*-2-fold crystal symmetry about *c* and the *quasi*-glide symmetry in the *a* direction.

Although **1** crystallizes in a triclinic lattice, the lattice parameters make it very close to monoclinic. Small reductions of both α and β (from 90.430 and 92.445, respectively) to 90° would result in a structure that, after suitable axis permutation, could be described in the space group $P2/c$, with the molecular 2-fold axes now coincident with the monoclinic 2-fold axes. This *pseudo*-symmetry can be seen clearly in Figure 3. The layers of molecules parallel to the 001 plane in the triclinic structure of **1** are all aligned very close to the crystal *c*-axis. The adjacent layer, related to the first by inversion symmetry, is also related by a *quasi*-glide plane parallel to the 001 plane and in the triclinic *a*-direction. This *pseudo*-monoclinic symmetry has unfortunate consequences for the determination of the crystal structure of **1**, as all the crystals examined were twinned by a 180° rotation about the *c** reciprocal axis (i.e., the perpendicular to the 001 plane, corresponding to the *b*-axis of the *pseudo*-monoclinic cell) with a concomitant high degree of overlap of reflections from the two domains. In most cases, additional twinning was also present, and the structure presented here was obtained from a carefully chosen crystal that only showed the 180° rotational twinning.

Crystals that contain large amounts of volatile solvent molecules in the lattice, such as **1** with seven methanols per Dy_3Fe_7 aggregate, usually lose some or all of this solvent rather rapidly on exposure of crystals to the air, with loss of crystallinity. However, crystals of **1**, although they do indeed lose all their lattice methanol molecules, remain crystalline. Using a synchrotron X-ray source, it was in fact possible to determine the crystal structure of a small desolvated crystal. The mosaicity was high, and diffraction to higher angles very weak, so that the full structure was not of publishable quality, but it was sufficient to show that the molecular structure is essentially unchanged, and to establish that a shearing of the fully solvated structure has resulted in a new unit cell (a = 14.447(2), b = 17.000(3), c = 21.277(3) Å, α = 108.962(14)°, β = 99.885(12)°, γ = 96.484(14)°, V = 4788.4(14) Å^3) in which the axis lengths and γ are largely unchanged, but α and β have both increased. The volume has decreased, as expected for loss of lattice solvent, and we formulate these crystals as the dihydrate on the basis of the microanalytic data. These crystals remain unchanged on exposure to air for at least a year.

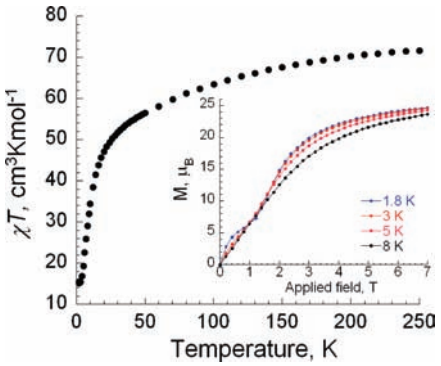

Figure 4. Temperature dependence of the χT product of **1**. Inset: Field dependence of the magnetization of **1**.

Magnetic Studies. Both static direct current (*dc*) and dynamic alternating current (*ac*) magnetic properties of **1** were studied on a polycrystalline sample dispersed in Apiezon grease. The χT product measured at 250 K and 0.1 T is 71.6 cm^3 K mol^{-1}, see Figure 4, a product that is in agreement[20] with the value of 73.135 cm^3 K mol^{-1} expected for seven high-spin Fe(III) ions with S = 5/2, g = 2, and C = 4.375 cm^3 K mol^{-1} and three Dy(III) ions with S = 5/2, L = 5, $^6H_{15/2}$, g = 4/3 and C = 14.17 cm^3 K mol^{-1}. Upon cooling, χT continuously decreases to reach a minimum of 15.1 cm^3 K mol^{-1} at 2 K and then slightly increases to 15.4 cm^3 K mol^{-1} at 1.8 K. This behavior is typically observed when both antiferromagnetic interactions between magnetic ions are dominant and the magnetic ground state corresponds to a ferrimagnetic arrangement of spins. Nevertheless, the thermal depopulation of the Dy(III) excited states, the Stark sublevels of the $^6H_{15/2}$ state,[21] may be partially responsible for the continuous decrease of χT below 30 K.

(20) Benelli, C.; Gatteschi, D. *Chem. Rev.* **2002**, *102*, 2369.
(21) (a) Kahn, M. L.; Sutter, J.-P.; Golhen, S.; Guionneau, P.; Ouahab, L.; Kahn, O.; Chasseau, D. *J. Am. Chem. Soc.* **2000**, *122*, 3413. (b) Kahn, M. L.; Ballou, R.; Porcher, P.; Kahn, O.; Sutter, J.-P. *Chem.—Eur. J.* **2002**, *8*, 525.

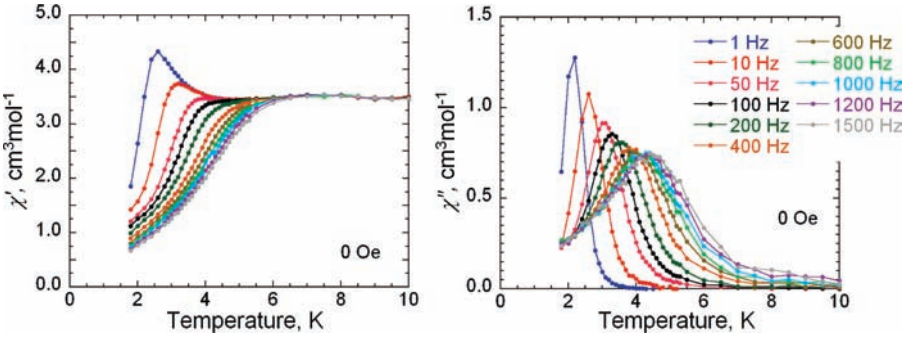

Figure 5. Temperature dependence of the in-phase, χ', left, and out-of-phase, χ'', right, components of the *ac* magnetic susceptibility, observed for **1** in a zero *dc* applied field.

A Curie−Weiss law fit of the 0.1 T magnetic susceptibility data of **1** between 100 and 250 K leads to an excellent linear fit with a Weiss temperature, θ, of −24.0 K, a Curie constant, C, of 72.84 cm^3 K mol^{-1}, and a corresponding effective magnetic moment, μ_{eff}, of 24.14 μ_B. The observed μ_{eff} moment is in excellent agreement with the 24.18 μ_B moment expected for three paramagnetic Dy(III) ions and seven Fe(III) ions with the S and g values given above. The negative θ indicates antiferromagnetic interactions between the spins within the cluster.

The magnetization measurements at low temperature obtained as a function of the field, see the inset to Figure 4, reveal that the magnetization increases between 1.8 and 8 K in two steps. First, between zero and 1 T applied field the magnetization increases rapidly, as expected for a non-zero spin ground state in **1**, before essentially leveling out to a step at about 7 μ_B at a field of 0.8 T. With further increase in applied field, the magnetization increases sharply again, with the gradient dM/dH reaching a maximum at about 1.6 T. Such an inflection is typically observed when the applied magnetic field overcomes antiferromagnetic interactions and aligns the spins in its direction, that is, low-lying excited states are progressively populated with an increase in the applied field. Since the spin ground state is difficult to define in a Dy(III) containing complex, it is also difficult to determine both the magnitude of the magnetic exchange interactions and the identity of the magnetic spins involved in the feature observed at 1.6 T. The magnetization curve then progressively flattens out, reaching 24.57 μ_B at 7 T, but without showing true saturation. The M vs H data also show the onset of hysteresis at 1.8 K, that is, a slow relaxation of the magnetization, with a very small coercive field of a few 100 μT (Supporting Information, Figure S2).

The relaxation of the magnetization in **1** was studied using *ac* susceptibility measurements both as a function of temperature at different frequencies and as a function of frequency at different temperatures. Slow relaxation of the magnetization is observed for **1** in a zero *dc* applied field (Figures 5 and Supporting Information, Figure S3) with a strong frequency dependence for both the in-phase, χ', and out-of-phase, χ'', susceptibility below 7 K. The maximum in χ'' is observed at 4.4 K at a frequency of 1500 Hz, with a shape- and frequency-dependence which strongly suggests that **1** behaves as a single molecule magnet. The characteristic relaxation time, τ, obtained

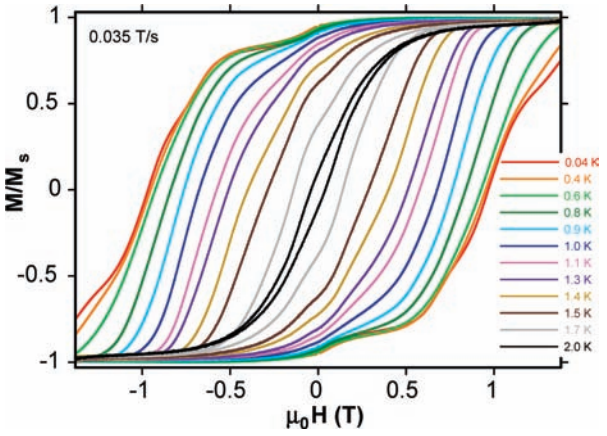

Figure 6. Normalized magnetization, M/M_s, versus *dc* applied field for single crystals of **1** obtained at the indicated temperatures at a fixed sweep rate of 0.035 T/s.

from both the temperature and frequency dependence of the out-of-phase susceptibility, χ'', exhibits exponential Arrhenius behavior, see Supporting Information, Figure S4, with a characteristic single molecule magnet energy barrier, U_{eff}, of 30.9 K and pre-exponential relaxation time, τ_0, of 1.3×10^{-7} s.

Subsequently, during the *ac* susceptibility measurements, a small *dc* field was applied to **1** to determine whether the relaxation rate would decrease because of the presence of a quantum relaxation pathway, see Supporting Information, Figure S5. The relaxation rate is almost unchanged, indicating that for **1**, at least above 1.8 K, there is no quantum tunneling of magnetization.

Magnetization measurements below 1.8 K were carried out on a single crystal of **1**, oriented with its magnetic easy-axis parallel with the applied magnetic field, using an array of micro-SQUIDs.[19] As is shown in Figure 6, these results confirm the presence of slow relaxation of the magnetization because hysteresis effects are clearly observed below 2 K at a field sweep rate of 0.035 T/s. The coercive field is both strongly temperature-dependent, increasing with decreasing temperature, and sweep-rate dependent, increasing with increasing sweep rate of the field, as would be expected for the superparamagnetic-like behavior observed for single molecule magnets. Below 0.5 K, the width of the hysteresis loop becomes temperature-independent at about 2 T for a 0.035 T/s sweep rate, indicating the presence of a quantum regime

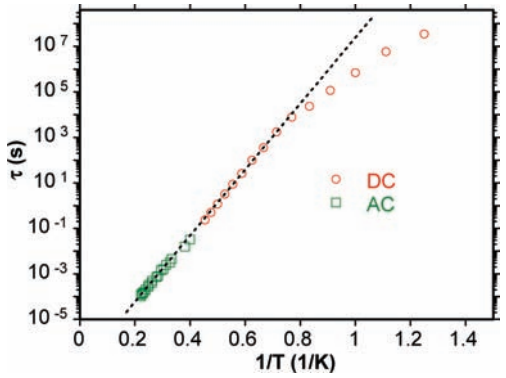

Figure 7. Arrhenius semilog plot of the relaxation time, τ, vs $1/T$ for a single crystal of **1** obtained between 0.8 and 5 K from *ac* susceptibility and *dc* magnetization decay measurements. The dashed line is a linear fit of the results obtained between 1.2 and 5 K, the thermally activated range of temperatures.

over which the relaxation of the magnetization occurs by quantum tunneling.

It should be noted that steps are also observed in the *M* vs *H* plots for **1**, that are probably the signature of the resonant quantum tunneling relaxation expected for a single molecule magnet. To obtain a more quantitative assessment of the dynamics of the magnetization relaxation, the *dc* magnetization decay was monitored as a function of time (Supporting Information, Figure S6). The resulting *dc* relaxation rate, together with the *ac* susceptibility reported above, have been combined and fit, see Figure 7, to obtain an effective energy barrier, U_{eff}, of 33.4 K and a relaxation time of 6.6×10^{-8} s for **1**.

Mössbauer Spectral Studies. The Mössbauer spectra of **1** obtained between 55 and 295 K are shown in Figure 8, and the spectra obtained between 3 and 15 K are shown in Figure 9.

The spectra indicate the absence of any magnetic sextet at 55 K and above, and the spectra have been analyzed with the superposition of six symmetric Lorentzian doublets assigned to the seven crystallographically inequivalent Fe(III) sites; two of these sites give rise to one doublet with twice the expected area, the doublet shown in red in Figure 8. The resulting fit parameters are six isomer shifts, six quadrupole splittings, one line width, as well as the total spectral area. If the seven crystallographic sites with degeneracy one have the same recoil free fraction at all temperatures, the expected relative areas of the six doublets are 1:2:1:1:1:1. Initial attempts to fit the spectra with this ratio indicated that the doublet shown in blue in Figure 8, with its low velocity peak at about −0.5 mm/s, has a relative area larger than expected, most likely because this iron site, Fe(1), has a larger recoil free fraction than the other sites. Hence, the relative areas of the doublets have been constrained to *x*:2:1:1:1:1. All the fits are excellent as is shown by the solid black total fit line in Figure 8. The total number of adjustable parameters used in the fits of the paramagnetic spectra is 15, specifically, six isomer shifts, six quadrupole splittings, one line width, the total absorption area, and one fractional area, *x*, for Fe(1). This number may seem rather large but all attempts to fit the spectra with fewer parameters and in a consistent way as a function of temperature between 3 and 295 K have failed.

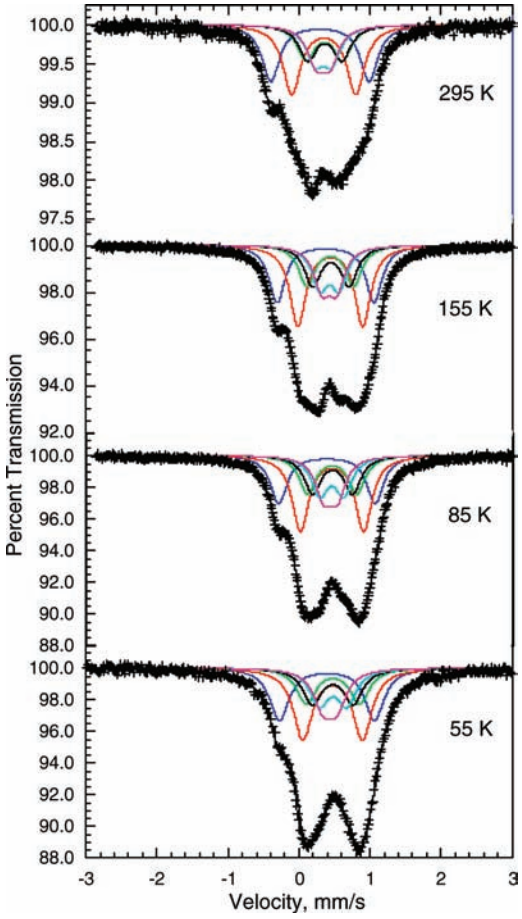

Figure 8. Mössbauer spectra of **1** obtained at the indicated temperatures. The black and color solid lines are the resulting fit and the six doublets used in the fit.

The initial estimate of the values for the isomer shifts and quadrupole splittings were such that the doublets are nested, that is, have very similar isomer shifts and different quadrupole splittings. The resulting hyperfine parameters, given in Table 2, confirm this initial choice, a choice that ensures that the isomer shifts are all reasonable for high-spin Fe(III) ions in an octahedral environment. This estimate is reasonable because the Fe(2)−Fe(7) *pseudo*-octahedral Fe(III) ions in **1** all have very similar average Fe−ligand bond distances, see Table 3, and thus will exhibit rather similar isomer shifts. In contrast, Table 3 reveals a range of distortions[22] for these Fe(III) environments, differing distortions that will lead to a range of quadrupole splittings.

The smallest isomer shift, δ_1, may be assigned to the Fe(1) site, which is the site that has a 5-fold coordination environment, an environment that also favors a tighter bonding and a larger recoil-free fraction. The doublet with a relative area of two may be assigned to the Fe(3) and Fe(5) ions because their crystallographic environment, bond distances, and the percentage bond distortions are very similar and give rise to one isomer shift and one quadrupole splitting. The remaining four doublets are assigned to Fe(2), Fe(4), Fe(6), and Fe(7) on the basis of their distortions; the assignments for the these sites

(22) Reger, D. R.; Gardinier, J. R.; Elgin, J. D.; Smith, M. D.; Hautot, D.; Long, G. J.; Grandjean, F. *Inorg. Chem.* **2006**, *45*, 8862.

given in Table 2 are tentative but probably valid. In Table 2, the hyperfine parameters and the relative area for the Fe(1) doublet and the average hyperfine parameters for the six remaining Fe(2)−Fe(7) doublets are reported.

Between 3 and 15 K the Mössbauer spectra of **1** result from the superposition of several sextets, as is shown in Figure 9. At 3 and 4.2 K the lines at −7, −4, and +8 mm/s, with a relative area of two, have been assigned to the Fe(3) and Fe(5) sites, whereas the lines at −5, −4, and +7 mm/s, with a relative area of one, have been assigned to Fe(1), because of its small isomer shift and large quadrupole interaction, parameters that result from its 5-fold coordination environment. The remaining portion of the spectral absorption has a relative area of four and has been

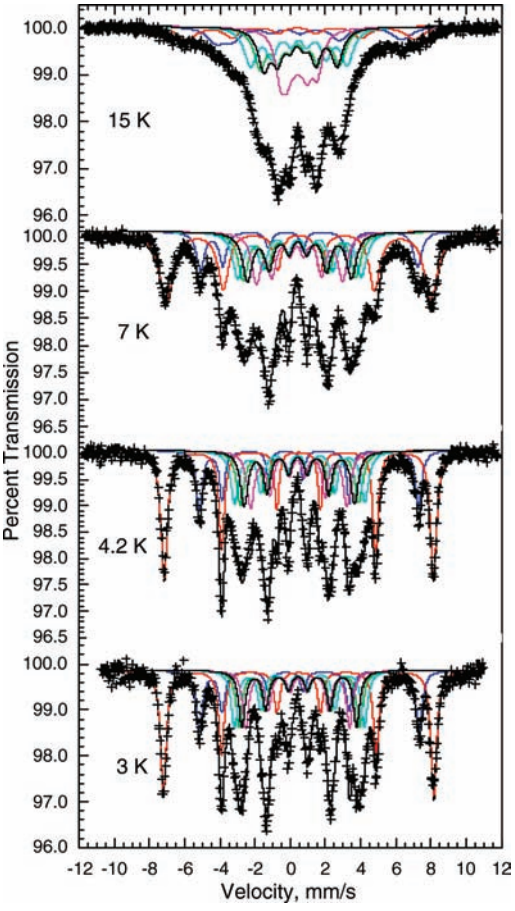

Figure 9. Mössbauer spectra of **1** obtained at the indicated temperatures. The black and color solid lines are the resulting fit and the six sextets used in the fit.

subdivided into four sextets, each with a relative area of one. Hence, fits with six sextets with initial relative areas of 1:2:1:1:1:1:1 have been carried out and the results are shown in Figure 9. All fit attempts with a smaller number of sextets were unsuccessful. In these fits, the six isomer shifts and the six quadrupole interactions were constrained to values that are in agreement with their temperature dependence in the paramagnetic region. The angles, θ, between the hyperfine field and the principal axis of the electric field gradient tensor have been adjusted, but the asymmetry parameter has been fixed at zero for all six sextets. Fits with one common line width for the six sextets were not as good and three line widths have been used, one for each of the outer sextets and one for the four inner sextets. The relative areas were fit in the last step of the fitting procedure, and they do not deviate significantly from 1:2:1:1:1:1:1, except at 8 and 15 K, temperatures at which the magnetic sextets are not fully developed.

The temperature dependence of the isomer shift, δ_1, and the weighted average of the five remaining isomer shifts is shown in Figure 10. The solid lines result from fits with the Debye model for the second-order Doppler shift, and the corresponding Mössbauer temperatures, Θ_M, are 541(12) and 445(11) K, respectively. The Mössbauer temperature for Fe(1) is higher than that for the other six iron sites because Fe(1) is more tightly bound in its 5-fold coordination site than the other six-coordinated iron ions. This larger Mössbauer temperature also justifies the larger relative area for Fe(1) as compared with the other sites above 55 K; at 3 and 4.2 K all the iron sites have equal recoil free fractions.

The temperature dependence of the six quadrupole splittings, ΔE_{Qi}, in **1** is shown in Figure 11; the temperature dependence of the Fe(1) quadrupole splitting and of the weighted average for Fe(2) to Fe(7) is shown in the inset to Figure 10. The quadrupole splitting of Fe(1) is larger than those of the six remaining iron ions because of its more distorted 5-fold environment. The quadrupole splittings show little dependence upon temperature between 3 and 295 K, as expected for high-spin Fe(III) ions for which the quadrupolar interaction arises only from a lattice contribution to the electric field gradient at the iron.

The temperature dependence of the six hyperfine fields observed in **1** is shown in the upper portion of Figure 12, and exhibits the usual decrease with temperature. A plot of the reduced hyperfine field for Fe(1), Fe(3)−Fe(5), and of the weighted average for the seven iron sites versus reduced temperature is shown in the lower portion of

Table 2. Mössbauer Spectral Parameters of **1**

T, K	relative area$_1$, %	δ_1,[a] mm/s	ΔE_{Q1}, mm/s	δ_{av},[a] mm/s	ΔE_{Qav}, mm/s	Γ, mm/s
295	0.205(5)	0.295(2)	1.383(7)	0.35(1)	0.54(3)	0.30(1)
225	0.199(4)	0.339(2)	1.365(5)	0.399(6)	0.54(1)	0.309(7)
155	0.184(2)	0.374(1)	1.367(2)	0.439(2)	0.579(4)	0.27(1)
85	0.172(2)	0.394(1)	1.358(3)	0.464(4)	0.593(9)	0.283(6)
65	0.171(4)	0.398(3)	1.346(8)	0.47(1)	0.62(2)	0.332(6)
55	0.161(4)	0.400(4)	1.337(9)	0.47(2)	0.61(4)	0.332(6)
15		0.400	1.337	0.47	0.63	
8		0.400	1.337	0.47	0.63	
4.2	0.161	0.400	1.337	0.47	0.63	

[a] The isomer shifts are relative to α-iron powder at 295 K.

Table 3. Iron(III) Coordination Environments in **1**

iron site	iron coordination environment	average iron bond distance, Å	standard deviation,[a] Å	iron bond distortion,[b] %
Fe(1)	NO_4	1.990(4)	0.133	4.53
Fe(2)	N_2O_4	2.037(4)	0.103	3.43
Fe(3)	N_2O_4	2.040(4)	0.114	3.98
Fe(4)	N_2O_4	2.050(4)	0.095	3.83
Fe(5)	N_2O_4	2.059(4)	0.102	3.99
Fe(6)	N_2O_4	2.047(4)	0.078	2.48
Fe(7)	N_2O_4	2.051(4)	0.076	2.63

[a] The standard deviation of the 5 or 6 average iron(III) bond distances. [b] The percentage iron bond distortions have been determined as explained in reference 22.

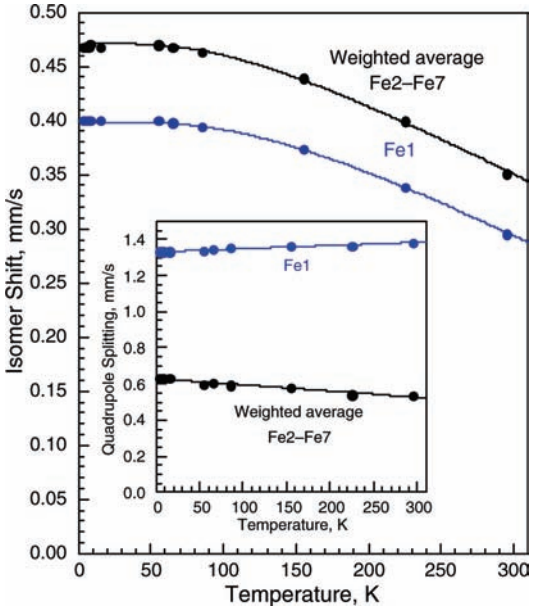

Figure 10. Temperature dependence of the isomer shift, δ_1, of Fe(1), blue circles, and the weighted average of the five remaining isomer shifts, black circles, in **1**. The solid lines are the result of a fit with the Debye model for the second-order Doppler shift.

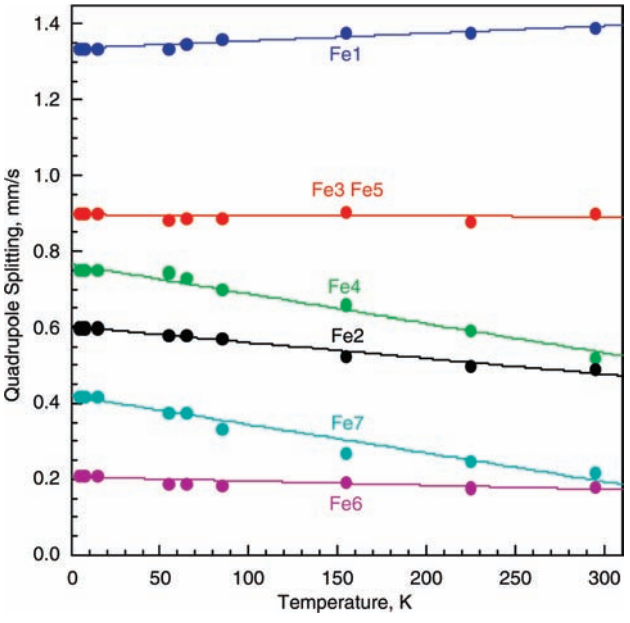

Figure 11. Temperature dependence of the six quadrupole splittings, $\Delta E_{Q\mathrm{i}}$, observed in **1**.

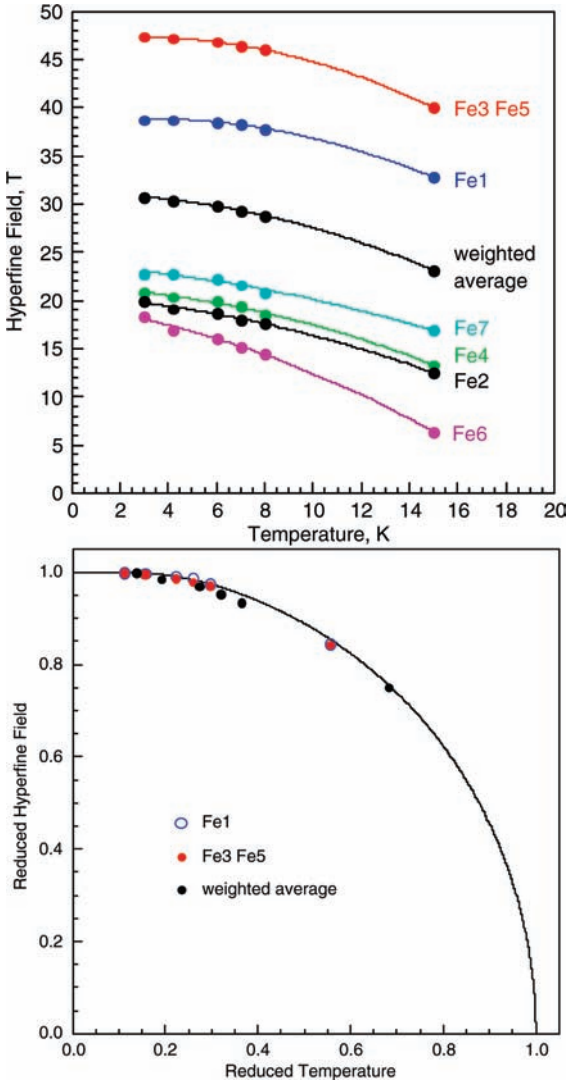

Figure 12. Temperature dependence of the six hyperfine fields, top, and the reduced hyperfine fields, for Fe(1), Fe(3)−Fe(5), and for the weighted average versus the reduced temperature in **1**, bottom. The critical temperature and saturation hyperfine field are 27 K and 38.8 T for Fe(1), 27 K and 47.4 T for Fe(3)−Fe(5), and 22 K and 30.8 T for the weighted average.

Figure 12. For this plot a critical temperature of 27, 27, and 22 K has been used for Fe(1), Fe(3)−Fe(5), and the weighted average, respectively. All three reduced fields follow the Brillouin curve for $S = 5/2$, shown as the solid black curve. Hence, from an initial Mössbauer spectral point of view, the Fe(III) ions in **1** appear to behave as expected in the presence of long-range magnetic order, an

ordering that occurs below about 40 K and is fully developed at 6 K and below. However, in view of both the magnetically dilute, relatively isolated, nature of the clusters found in **1** and the barrier to the relaxation of the magnetization noted above, this is not the case as will be shown below.

The analysis of the Mössbauer spectra must be consistent with the magnetic results described above. The relaxation times of the magnetization of **1** at 4.2, 15, 35, and 55 K are about 190×10^{-6}, 0.61×10^{-6}, 0.17×10^{-6}, and 0.12×10^{-6} s, as obtained from the Arrhenius parameters derived from the *dc* and *ac* susceptibilities, see Figure 7. The Larmor precession time for the iron-57 nuclear magnetic moment in a magnetic field of 30 T is about 0.05×10^{-6} s. Hence, at 3, 4.2, and 6 K the magnetization relaxation time is about 10^4 to 10^3 times larger than the Larmor precession time, and fully developed sextets with sharp lines are observed. At 35 and 55 K, the magnetization relaxation times are between four and two times the Larmor precession time, and somewhat broadened and slightly broad sextets are observed at 35 and 45 K, respectively, see Figure 13, indicating a decrease in the relaxation time of the magnetization. However, the observed Mössbauer spectra do not show the characteristic temperature dependence of the hyperfine fields in the presence of slow paramagnetic relaxation, that is, a sudden appearance of a saturated hyperfine field at a temperature corresponding to a relaxation time similar to the Larmor precession time. In the Mössbauer spectra of the Fe_4, Fe_8, and Fe_{13} clusters, this typical behavior in the presence of slow paramagnetic relaxation was observed.[23,24] A Mössbauer spectral study[25] of dinuclear lanthanide-iron systems also shows spectra broadened by slow relaxation at 4.2 K and sharp doublets at 295 K. In contrast in **1**, the Brillouin behavior of the hyperfine fields indicates that there is coherent alignment of the spins within the cluster, or at least within an estimated distance of 15 Å, the approximate distance between the centers of the two clusters present in the unit cell. It has previously been observed[26] that ^{57}Fe Mössbauer spectra exhibit fully developed sharp sextets in the presence of short-range magnetic correlations within a distance of 50 Å. It seems that in the present case, the intracluster magnetic correlations within the about 2600 Å^3 volume of the decanuclear cluster of **1** are sufficient to yield sharp sextets. The use of the volume of the decanuclear cluster to quantify the dimension of the cluster that gives rise to coherent alignment of spins is rather arbitrary but the distance between the two Fe(1) central iron(III) ions in the unit cell is a good estimate of the distance giving rise to the magnetic correlations, and the 10 magnetic centers in the cluster must be included in an estimate of the volume.

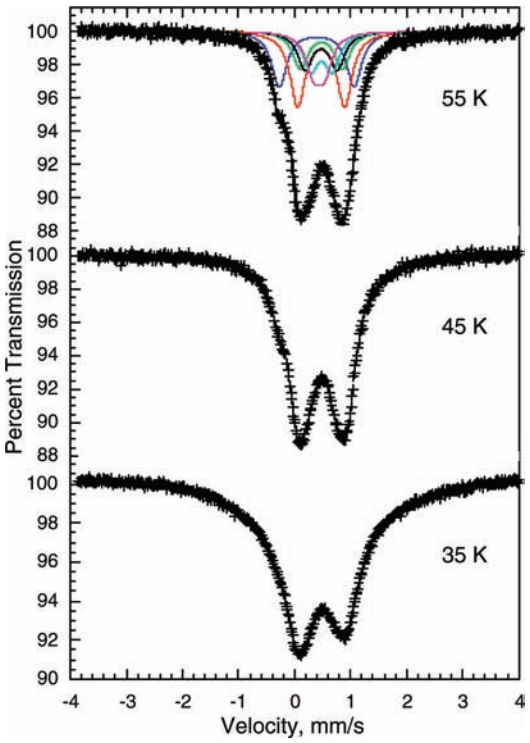

Figure 13. Mössbauer spectra of **1** showing the onset of slow relaxation broadening at 35 K, a slight broadening at 45 K, and paramagnetic behavior at 55 K.

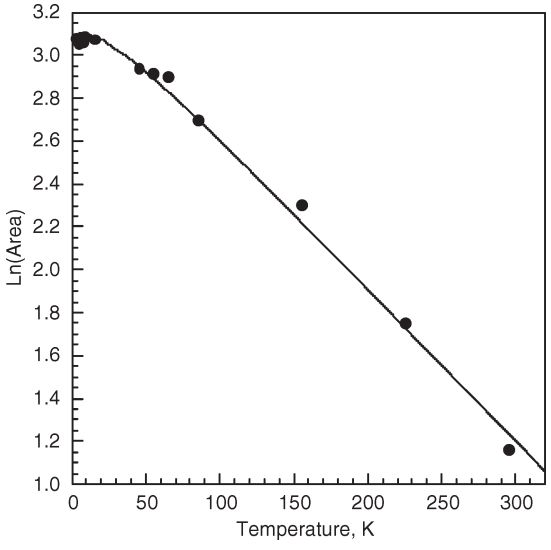

Figure 14. Temperature dependence of the logarithm of the spectral absorption area in **1**. The solid line is the result of a fit with the Debye model.

The temperature dependence of the logarithm of the total Mössbauer spectral absorption area is shown in Figure 14. The solid line is a fit with the Debye model, and the resulting Debye temperature, Θ_D, a temperature similar to the Debye temperature, is 137(2) K. As is usually observed, this temperature is smaller than the Mössbauer temperature obtained from the temperature dependence of the isomer shift, a dependence that is more sensitive to high-frequency phonons than that of the absorption area.[26]

(23) (a) Cianchi, L.; Del Giallo, F.; Spina, G.; Reiff, W.; Caneschi, A. *Phys. Rev. B* **2002**, *65*, 064415. (b) Cianchi, L.; Spina, G. In *NMR-MRI, μSR and Mössbauer spectroscopy in Molecular Magnets*; Springer: Milan, 2007; Part III, pp 277−293.
(24) van Slageren, J.; Rosa, P.; Caneschi, A.; Sessoli, R.; Casellas, H.; Ratikin, Y. V.; Cianchi, L.; Del Giallo, F.; Spina, G.; Bino, A.; Barra, A.-L.; Guidi, T.; Caretta, S.; Caciuffo, R. *Phys. Rev. B* **2006**, *73*, 014422.
(25) Figuerola, A.; Tangoulis, V.; Sanakis, Y. *Chem. Phys.* **2007**, *334*, 204.
(26) Carling, S. G.; Hautot, D.; Watts, I. D.; Day, P.; Visser, D.; Ensling, J.; Gütlich, P.; Long, G. J.; Grandjean, F. *Phys. Rev. B* **2002**, *66*, 1044407.

Conclusions

The reaction of *N*-methydiethanolamine, $mdeaH_2$, and benzoic acid with $FeCl_3$ and $DyCl_3$ yields a decanuclear coordination cluster, $[Dy_3Fe_7(\mu_4\text{-}O)_2(\mu_3\text{-}OH)_2(mdea)_7(\mu\text{-}benzoate)_4(N_3)_6]\cdot 2H_2O\cdot 7CH_3OH$, **1**, that crystallizes in the space group $P\bar{1}$ with $Z = 2$. The structure of **1** has three and seven crystallographically distinct Dy(III) and Fe(III) ions; six of the Fe(III) ions are *pseudo*-octahedrally coordinated, whereas the seventh has a trigonal bipyramidal coordination geometry. The three intercluster Dy(III)−Dy(III) distances within the unit cell range from 10.99 to 16.68 Å whereas the seven Fe(III)−Fe(III) distances range from 9.16 to 19.32 Å and, as a consequence, intermolecular exchange coupling is either weak or absent. Macroscopic *dc* and *ac* magnetic susceptibility studies indicate that intracluster antiferromagnetic interactions between the Dy(III) and Fe(III) ions in **1** are dominant, and yield a ferrimagnetic arrangement of spin carriers. Both *ac* χ' and χ'' susceptibilities measured on a powder sample, and single crystal magnetization studies, reveal that **1** undergoes a slow relaxation of its magnetization. The effective energy barrier, U_{eff}, of 33.4 K for this relaxation is the highest yet reported for a lanthanide(III)-Fe(III) single molecule magnet and the second highest energy barrier yet reported for a 3d-4f single molecule magnet. Although many Fe(III)-based single molecule magnets are known,[27] it is likely that the height of the energy barrier in **1** mainly results from the single-ion anisotropies of the Dy(III) ions, as we have previously demonstrated for Mn(III)−Dy(III) single molecule magnets.[5f]

(27) (a) Wieghardt, K.; Pohl, K.; Jibril, I.; Huttner, G. *Angew. Chem., Int. Ed. Engl.* **1984**, *23*, 77. (b) Powell, A. K.; Heath, S. L.; Gatteschi, D.; Pardi, L.; Sessoli, R.; Spina, G.; Del Giallo, F.; Pieralli, F. *J. Am. Chem. Soc.* **1995**, *117*, 2491. (c) Goodwin, J. C.; Sessoli, R.; Gatteschi, D.; Wernsdorfer, W.; Powell, A. K.; Heath, S. L. *J. Chem. Soc., Dalton Trans.* **2000**, 1835. (d) Accorsi, S.; Barra, A.-L.; Caneschi, A.; Chastanet, G.; Cornia, A.; Fabretti, A. C.; Gatteschi, D.; Mortal, C.; Olivieri, E.; Parenti, F.; Rosa, P.; Sessoli, R.; Sorace, L.; Wernsdorfer, W.; Zobbi, L. *J. Am. Chem. Soc.* **2006**, *128*, 4742.

The Mössbauer spectra of **1** obtained between 55 and 295 K are characteristic of paramagnetic behavior and exhibit six partially resolved Fe(III) quadrupole doublets, in the ratio of *x*:2:1:1:1:1, that may be assigned to the trigonal bipyramidal Fe(1) site, the *pseudo*-octahedral Fe(3) and Fe(5) sites, and to the four remaining *pseudo*-octahedral sites.

An indication of Mössbauer spectral broadening in **1** because of the onset of slow magnetic relaxation is first observed upon cooling to 45 K, becomes more apparent at 40 K, and is obvious at 35 K. The spectra of **1** obtained between 3 and 35 K are consistent with the presence of Fe(III) intracluster antiferromagnetic coupling with slow relaxation of the magnetization relative to the Larmor precession time, thus confirming, on a microscopic scale, the presence of a barrier to the magnetic relaxation below 35 K.

Acknowledgment. The authors acknowledge with thanks the financial support of the DFG (Grant SPP 1137 and Center for Functional Nanostructures), QuEMolNa (MRTN-CT2003-504880), MAGMA-Net (NMP3-CT-2005-515767) and Fonds National de la Recherche Scientifique, Belgium, through Grants 9.456595 and 1.5.064.05.

Supporting Information Available: Crystallographic data for **1** in CIF format. dM/dH vs H and magnetization obtained at 1.8 K, frequency dependence of the in-phase, χ', and out-of-phase, χ'', components of the *ac* magnetic susceptibility obtained for **1** in a zero *dc* applied field, Arrhenius semilog plot of τ vs $1/T$ obtained from *ac* susceptibility measurements, frequency dependence of the in-phase, χ', and out-of-phase, χ'', components of the *ac* magnetic susceptibility measured in different *dc* applied fields and at 3.8 K and the reduced magnetization, M/M_s vs time decay obtained at zero *dc* applied field for a single crystal of **1**. This material is available free of charge via the Internet at http://pubs.acs.org.